

# Alongshore winds force warm Atlantic Water toward Helheim Glacier in southeast Greenland

T. Snow<sup>1,2,3</sup>, W. Zhang<sup>4</sup>, E. Schreiber<sup>5</sup>, W. Abdalati<sup>2,3</sup>, T. Scambos<sup>2</sup>

<sup>1</sup>Colorado School of Mines, Department of Geophysics, Golden, CO, USA

<sup>2</sup>Cooperative Institute for Research in Environmental Sciences, University of Colorado, Boulder, CO, USA

<sup>3</sup>University of Colorado Boulder, Geography Department, Boulder, CO, USA

<sup>4</sup>Applied Ocean Physics and Engineering Department, Woods Hole Oceanographic Institution, Woods  
Hole, MA, USA

<sup>5</sup>UNAVCO, 6350 Nautilus Drive, Boulder, CO, 80301, USA

## Key Points:

- Alongshore wind-driven coastal upwelling near Sermilik Fjord drives intrusions of Atlantic Water onto the continental shelf
- Intrusions often lead to warmer subsurface water in the inner shelf and fjord
- Less transport within the East Greenland Coastal Current makes fjords more susceptible to Atlantic Water intrusions

---

Corresponding author: Tasha Snow, [tasha.snow@colorado.edu](mailto:tasha.snow@colorado.edu)

**Abstract**

Enhanced transport of warm subsurface Atlantic Waters (AW) into Greenland fjords has driven glacier mass loss, but the mechanisms transporting AW to the fjords remain poorly characterized. Here, we identify a wind-driver for AW inflow toward Sermilik Fjord abutting Helheim Glacier, one of Greenland's largest glaciers. Often associated with the passing of cyclones and subsequent sea surface lowering, a weakening or reversal of north-easterly alongshore winds stimulates coastal ocean upwelling that, through interactions with Sermilik's bathymetric trough on the continental shelf, leads to enhanced AW upwelling and inflow along the trough. These intrusions produce ocean warming at deep moorings near Sermilik Fjord mouth ( $0.31\pm 0.18^\circ\text{C}$ ) and within the fjord (250m:  $0.30\pm 0.19^\circ\text{C}$ ; 350m:  $0.17\pm 0.09^\circ\text{C}$ ) that is not diminished by subsequent coastal downwelling. Similar wind-driven processes at other bathymetric trough regions around Greenland may play a substantial role in ocean heat transport towards much of the Greenland Ice Sheet.

**Plain Language Summary**

Higher transport of the warm subtropical Atlantic Waters into Greenland fjords has driven glacier mass loss, but the mechanisms transporting the subtropical waters to glacier fronts remain poorly characterized. In this work, we identify a wind mechanism for transporting subtropical water towards Helheim Glacier, one of Greenland's largest glaciers. Often associated with the passing of cyclones, alongshore wind events stimulate ocean circulation that brings subtropical waters from offshore onto the continental shelf along a submarine trough that leads to Helheim. Our measurements show that when these events produce ocean warming near-shore, they may help to transport more heat to Helheim Glacier front where it can cause enhanced ice melting. A higher number of wind events in a season has the potential to impact glacier calving, thinning, and retreat. These events may also occur along other bathymetric troughs leading toward Greenland glaciers and, therefore, may be important for predicting future Greenland Ice Sheet ice loss.

**1 Introduction**

The Greenland Ice Sheet is now the leading contributor to global sea level rise each year and approximately half of this mass loss results from outlet glacier dynamics (speedup, thinning, and retreat) at its periphery (Enderlin et al., 2014; Mougnot et al., 2019; IM-BIE Team, 2019; Smith et al., 2020). Helheim Glacier - one of the largest glacier in Greenland - has experienced multiple dynamic ice loss events over the past two decades, as have other neighboring glaciers in southeastern Greenland (Howat et al., 2008; Murray et al., 2010). These regionally synchronous events were likely triggered by enhanced submarine melting by the ocean; acceleration, thinning, and retreat at Helheim corresponded to warming waters and enhanced ocean heat transport into Sermilik Fjord, the fjord that abuts Helheim (Holland et al., 2008; Mougnot et al., 2015; Millan et al., 2018). It is unclear, however, what mechanisms modulate that ocean heat transport from the broader ocean into the fjords through time and, thus, what may have triggered the past glacier retreat events.

57 Transport of relatively warm (2.0-5.2°C) Atlantic-origin subsurface waters (AW;  
58 found from 150-250 m to the seafloor) delivers much of the ocean heat to Helheim Glacier  
59 front and can vary substantially as a result of highly variable ocean circulation (Straneo  
60 et al., 2010; Jackson et al., 2014). Within Sermilik Fjord, relatively cold ( $<4^{\circ}\text{C}$ ) and fresh  
61 Polar-origin water (PW) resides at the surface above AW in a two-layer circulation struc-  
62 ture (Straneo et al., 2010; Sutherland et al., 2014). The dominant mode for variability  
63 within these layers is an oscillatory "intermediary" circulation caused by wind-driven coastal  
64 geostrophic currents and changing offshore water mass properties (Svendsen & Thomp-  
65 son, 1978; Straneo et al., 2010; Jackson et al., 2014; Fraser et al., 2018). Under this highly  
66 dynamic circulation scheme, alongshore northeasterly (prevailing) winds drive Ekman  
67 transport shore-ward at the surface and create a compensating flow offshore at depth  
68 (Håvik & Våge, 2018), resulting in coastal ocean downwelling (Figure 1b). During such  
69 downwelling, the sea surface height can rise  $\sim 15$  cm (Jackson et al., 2014; Cowton et al.,  
70 2016), isopycnals heave downwards (Straneo et al., 2010; Jackson et al., 2014), and the  
71 PW layer thickens. Opposing southwesterly winds drive the opposite set of changes (Fig-  
72 ure 1c). Ocean pressure gradients between the coastal waters and the fjord, created by  
73 coastal downwelling or upwelling, drive rapid current reversals within intermediate lay-  
74 ers of Sermilik Fjord on synoptic timescales of 4-10 days (Jackson et al., 2014). These  
75 intermediary currents can be strong enough to flush the upper 300 m of the fjord within  
76  $\sim 4$  days if persistent and therefore have the potential to drive large water and heat ex-  
77 changes with the shelf (Straneo et al., 2010; Sciascia et al., 2014). The wind-driven cir-  
78 culation sometimes leads to changed water properties within the fjord, but can also re-  
79 sult in oscillations with no net change in water properties (Jackson et al., 2018). It is  
80 unclear what distinguishes these two.

81 Outside the fjord, a complex circulation system allows AW to intrude onto the con-  
82 tinental shelf ( $\sim 300$ - $400$  m deep) along a bathymetric trough ( $\sim 15$  km wide,  $\sim 400$ - $900$   
83 m deep) that leads to Sermilik Fjord and Helheim (Figure 1b,c; Sutherland et al., 2013;  
84 Harden et al., 2014; Snow et al., 2021). The East Greenland Coastal Current (EGCC)  
85 flows at the surface along the coast carrying PW equatorward (Sutherland & Pickart,  
86 2008), and AW spreads onto the shelf beneath it. Offshore, the Irminger Current (IC)  
87 carries AW southward throughout the upper 500 m (Rudels et al., 2002; Johannessen  
88 et al., 2011; Våge et al., 2011; Andresen et al., 2012), which can be diverted onto the shelf  
89 (Sutherland et al., 2013; Harden et al., 2014; Snow et al., 2021). Aside from general in-

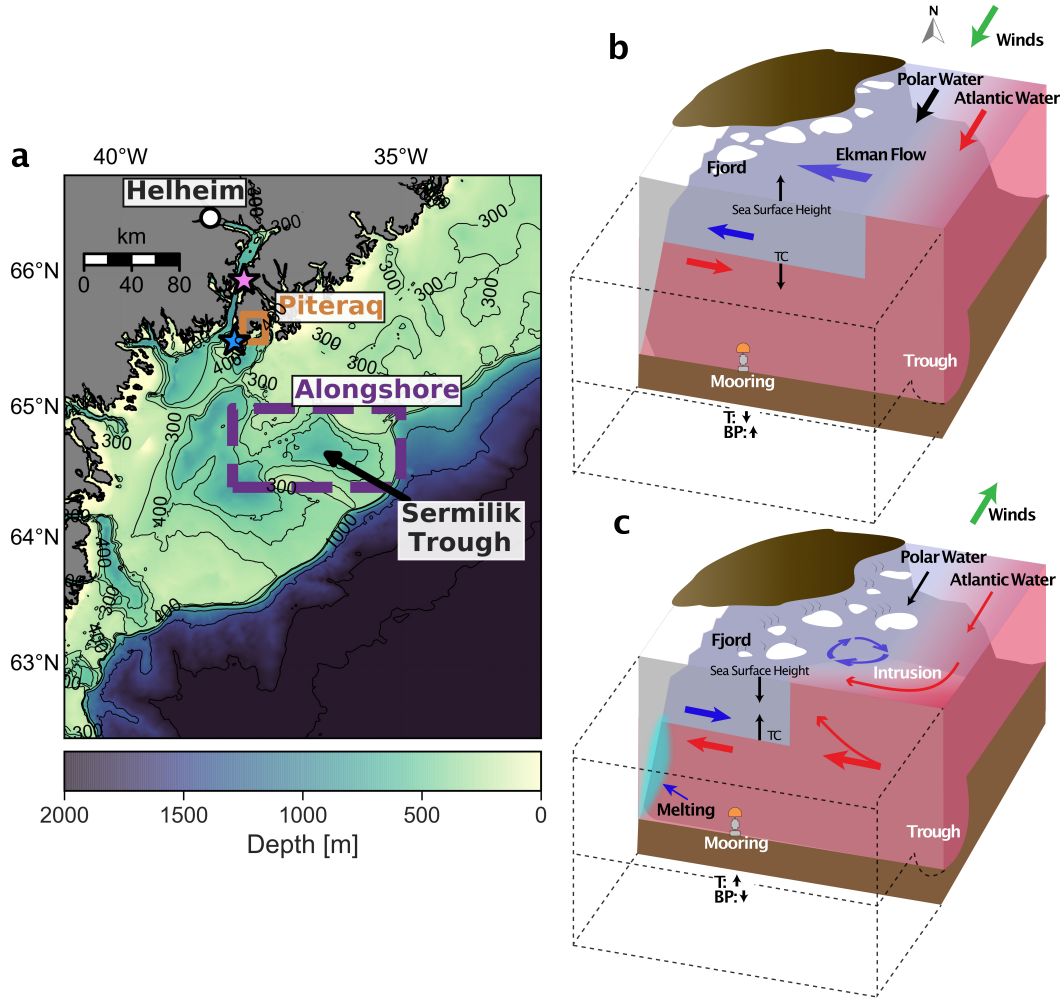


**Figure 1.** The Sermilik Trough study region and wind-driven ocean circulation along the trough. (a) Bathymetry for the continental shelf near Sermilik Fjord and Trough. Sampling locations for the ERA-5 reanalysis alongshore winds (purple dashed) and piteraq (orange) are shown (see Methods). Stars indicated the shelf (blue) and mid-fjord (pink) mooring locations. Bathymetry is from BedMachine v3 with the thin black lines representing contours at 300, 400, 500 m, and every 500 m thereafter (Morlighem et al., 2017). (b,c) Also shown are schematics of the ocean circulation along Sermilik Trough during winds favoring (b) downwelling and (c) upwelling. Arrows indicate Polar Water (blue) and Atlantic Water (red) flow direction. Clockwise-rotating purple arrows indicate the vorticity created by coastal-trapped waves, which stimulates Atlantic Water intrusion along the trough. White and brown features indicate ice and land, respectively. We use the following abbreviations: TC (thermocline), BP (bottom pressure), and T (temperature).

90 flow at depth, full-depth AW inflow occurs on synoptic timescales along the trough or  
 91 as seasonally-varying inflow across portions of the shelf. AW intrudes further onto the  
 92 shelf in the fall and is associated with a narrower EGCC banked up against the coast

93 (Harden et al., 2014; Snow et al., 2021). Intrusions of AW may be linked with EGCC  
94 transport variability (Murray et al., 2010), cyclonic eddies (Bruce, 1995; Sutherland &  
95 Pickart, 2008; Sutherland et al., 2013), tidal variability, or fluctuations in alongshore winds  
96 (Hampson, 2020). However, little work has been done in the shelf region to link the broader  
97 ocean and fjord during these events, so the drivers of the intrusions and linkages to wa-  
98 ter property changes inshore remain unclear.

99 Here, we use MODIS optical imagery and sea surface temperatures (SST) from the  
100 continental shelf region near Sermilik Fjord to characterize intrusions of AW, their drivers,  
101 and how they impact shelf and fjord subsurface water temperatures. Unlike previous work  
102 on AW variability within Sermilik Fjord and near the fjord mouth, we produce a com-  
103 prehensive shelf-wide study of AW intrusion and its variability from 2010-2013 when we  
104 have coincident moored ocean observations. We investigate mechanisms driving these  
105 intrusions using ECMWF (European Center Medium-Range Weather Forecasts) reanal-  
106 ysis data, sea surface height, and SST-derived EGCC variability. We show that coastal  
107 upwelling, often caused by upwelling-favorable winds generated by the passing of a cy-  
108 clone and subsequent sea surface height lowering, drive these intrusions. We use moored  
109 subsurface ocean temperature records from the continental shelf and fjord to determine  
110 the impacts that the intrusions have on subsurface ocean temperatures that may even-  
111 tually reach Helheim Glacier. Our findings suggest that an interplay between EGCC trans-  
112 port and wind variability plays a large role in ocean heat transport into Sermilik Fjord,  
113 and potentially other fjords in southeastern Greenland.

## 114 **2 Background**

115 A timeseries of MODerate Resolution Imaging Spectroradiometer (MODIS) opti-  
116 cal images from February 27th to March 4th, 2013 reveals the evolution of a rapid AW  
117 intrusion cross-cutting from the slope to inner continental shelf near Sermilik Fjord (Fig-  
118 ure 2a). The intrusion bisected the EGCC, which was, at the time, choked with seasonal  
119 sea ice, making the intrusion observable with optical imagery. Just before the intrusion  
120 on February 27th, sea ice hugged the coast flowing to the south under prevailing north-  
121 easterly winds that had persisted for most of the preceding seventeen days according to  
122 ECMWF reanalysis data. Clouds from two cyclonic systems passing by late on Febru-  
123 ary 27th and 28th precluded visibility of the surface, but winds shifted early on Febru-  
124 ary 28th briefly and again March 1st to blow at  $\sim 10$  m/s from a northwesterly direction

125 (250° to 350°) off the ice sheet, where they remained for the next two days. In imagery  
126 from the afternoon of March 1st, the intrusion had snaked across >40 km of the EGCC  
127 within the last two days bringing AW from the offshore IC almost to the mouth of Ser-  
128 milik Fjord along the northeastern flank of the Sermilik Trough. Observed through MODIS  
129 Band 31 (thermal infrared)-derived brightness temperatures, portions of the AW intru-  
130 sion were  $\sim 4^\circ\text{C}$  warmer than surrounding EGCC and fjord waters (Figure S1c). March  
131 2nd imagery (Figure 2a) shows the remnants of the intrusion being encroached upon by  
132 sea ice within the EGCC and surface outflow from Sermilik Fjord, both moving to the  
133 south with the current. By the 4th when winds returned to their prevailing northerly  
134 direction, sea ice had been pushed southward covering the Sermilik Trough region, and  
135 the cross-shelf intrusion was no longer visible. This phenomenon has not been previously  
136 studied, and its influence has not been accounted for in large-scale models. Intrusions  
137 of this kind may rapidly advect AW and heat into Sermilik Fjord and toward Helheim  
138 Glacier and may therefore serve as an important factor in glacier dynamics (Figure 1c).

## 139 **Data and Methods**

140 AW intrusions are observable throughout the MODIS record near Sermilik Fjord,  
141 and they appear to vary widely in size and extent. To characterize these intrusions and  
142 determine their frequency and variability in time, we initially identify AW intrusion events  
143 along the Sermilik Trough using MODIS optical imagery from NASA WorldView (see  
144 Table S1, Figure 2a). The intrusions were selected from a larger set in the observable  
145 record to be clearly illustrative of the processes involved, and are identified by both the  
146 ice-free water cross-cutting the EGCC, as well as the surface outflow from fjords (i.e. open  
147 water streaming to the south) that follows. We make these observations from 2010 to  
148 2013 when simultaneous moored temperature records exist for the region, and only for  
149 January through June when sea ice cover along the EGCC makes the intrusions read-  
150 ily identifiable in the visible spectrum. Optical identification of the intrusions restricts  
151 our observations to AW intrusions that have surface expressions; therefore, intrusions  
152 that do not fully penetrate to the surface are unobserved. Further, cloud cover frequently  
153 obscures observations of the ocean surface. Thus, our observations include only a frac-  
154 tion of the total intrusion events during the study period, but the available data sets sup-  
155 port a clear characterization of the processes.

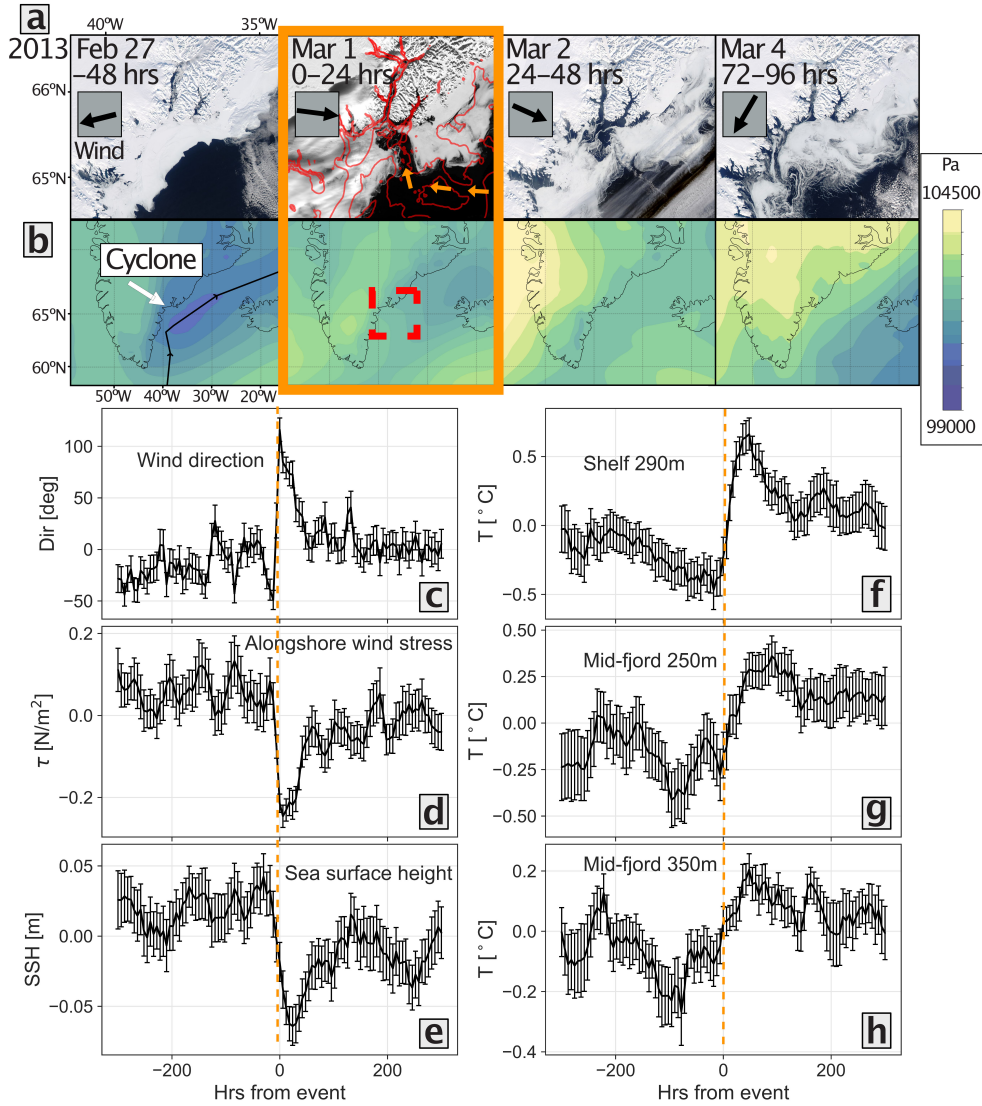


**Figure 2.** Evolution of Atlantic Water (AW) intrusions near Sermilik Fjord. (a) MODIS optical imagery of an AW intrusion from Feb 27th to Mar 4th, 2013. Hours refers to hours before (negative) or since (positive) the shifting of alongshore wind stress and initiation of the intrusion (orange). Wind direction and relative speed are depicted by the arrows within gray boxes. The red contours indicate the 250 m and 500 m isobaths, which show the location of Sermilik Trough. Orange arrows indicate the right-hand side of the trough and the path of AW shown in Figure S1. (b) Mean sea level pressure for each time step. A cyclone is shown with the black lines indicating the cyclone track. The red box indicates the location of the images in panel (a). (c-h) Composites of atmospheric and ocean parameters during fifty-three (53) identified AW intrusion events (see Results): (c) ERA-5 wind direction, (f) alongshore wind stress (positive means northeasterly), (e) sea surface height (SSH), and mooring temperatures from (f) the continental shelf near Sermilik Fjord mouth (290 m) and mid-fjord at (g) 250 m and (h) 350 m depth. The onset of negative alongshore wind forcing is shown by the orange lines, and hours are the same as in (a).

156           Synoptic-scale ocean circulation in the Sermilik Trough region may have ties to weather  
157 conditions, such as wind patterns. Previous work in Sermilik Fjord (Straneo et al., 2010;  
158 Jackson et al., 2014, 2018) and along the southeastern coast of Greenland (Sutherland  
159 & Pickart, 2008; Oltmanns et al., 2014; Le Bras et al., 2018) has shown strong correla-  
160 tions between ocean circulation patterns and various wind drivers, including cyclones and  
161 piteraqs (hurricane intensity downslope winds in the off-shore direction), supporting the  
162 notion that winds may influence these intrusions. Here we investigate the influence of  
163 atmospheric variability on the intrusions using atmospheric reanalysis data from the ECMWF  
164 ERA-5 operational reanalysis data set (Copernicus Climate Change Service (2017) ERA-  
165 5). From ERA-5, we use the 6-hourly 2-m wind field, instantaneous turbulent surface  
166 stresses, and mean sea level pressure fields to determine the atmospheric variability be-  
167 fore and after the intrusions. From the ERA-5 U and V wind speeds and stress, we cal-  
168 culate the northeasterly alongshore wind at the shelf break (Figure 1a; see Supplemen-  
169 tal Information). A positive alongshore northeasterly wind component specifies downwelling-  
170 favorable winds along the coast; a negative southwesterly wind specifies upwelling. To  
171 investigate the influence of cyclones, cyclone frequency and tracks are derived from ERA-  
172 5 records using an advanced cyclone detection and tracking algorithm as described in  
173 Crawford and Serreze (2016) and Crawford et al. (2020). Piteraqs (or Downslope Wind  
174 Events) were identified following Oltmanns et al. (2014) (Figure 1a; see Supplementary  
175 Information).

176           We investigate the extent to which intrusions affect ocean properties nearshore and  
177 within Sermilik Fjord by examining ocean temperature changes and sea surface height  
178 (SSH) during the intrusions. We use mooring temperature data from the continental shelf  
179 within the trough leading to Sermilik Fjord and within the fjord (Figure 1a), which were  
180 both deployed multiple times between August 24, 2009 - August 18, 2013 (see Supple-  
181 mentary Information; Jackson et al., 2014; Harden et al., 2014; Jackson & Straneo, 2016).  
182 The shelf mooring was deployed  $\sim 290$  m depth near the mouth of Sermilik Fjord. We  
183 also use SSH records from Harden et al. (2014), which were calculated from bottom pres-  
184 sure measurements at the same shelf mooring. The mooring within the fjord was located  
185 mid-fjord - 32 km from the shelf mooring and  $\sim 70$  km from the Helheim Glacier front  
186 - at  $\sim 250$ ,  $\sim 350$ ,  $\sim 400$ , and  $\sim 550$  m depth. These moorings provide a time varying record,  
187 averaged to 6-hourly time steps, of subsurface AW that is known to flow onto the con-  
188 tinental shelf and into Sermilik Fjord (Straneo et al., 2011; Jackson & Straneo, 2016) and

189 would likely detect ocean property changes associated with the variability of AW intru-  
190 sions at depth.

191 Prominence of the EGCC may also affect intrusion of AW onto the continental shelf  
192 (Murray et al., 2010). To investigate this possibility, we obtain the width of the EGCC  
193 during the intrusions using MODIS SST-derived observations of PW extent based on Snow  
194 et al. (2021) with small refinements (see Supplementary Information).

## 195 **Results**

196 We visually identified fifty-three (53) intrusion events during winter and spring (Jan-  
197 uary to June) between 2010 and 2013 (see Table S1, Figure S2). All intrusions are marked  
198 by ice-free waters – warmer than the surrounding EGCC and fjord surfaces – cutting through  
199 the sea ice covered EGCC along Sermilik Trough. We interpret these as an inflow of AW  
200 at the surface. In several of the more distinct intrusions, cross-shelf velocities of the in-  
201 trusion flow were 0.13-0.19 m/s based on the distance that the intrusions crossed within  
202 a 24-hour period (e.g., 10.9-16.2 km for May 20, 2010 and March 26, 2010, respectively).  
203 Within 24-48 hours after the intrusion becomes visible, outflow at the surface is indicated  
204 by outward spreading of sea ice and cool PW away from the coast except along the trough,  
205 and by relatively ice-free waters flowing out of Sermilik Fjord to the south within the  
206 EGCC.

207 Shifts in alongshore wind velocity and SSH preceded, and appear to drive, the AW  
208 intrusion events (Figure S2). Intrusions most frequently occurred after the passing of a  
209 low pressure (LP) system (87% of selected intrusions) and less frequently with only a high  
210 pressure (HP) system nearby (11%). Winds during most of the intrusion events took two  
211 forms within the 24 hours preceding the intrusions: i) winds that shifted from the pre-  
212 vailing northeasterly direction to a westerly direction, and ii) winds that weakened fol-  
213 lowing strong northeasterly wind stresses (typically  $>15$  m/s; Figure S2); the latter oc-  
214 curred less frequently (13 of the events). Intrusions also often coincided with a drop in  
215 SSH. These wind and SSH patterns are consistent with a transition from a wind-driven  
216 coastal downwelling regime – building sea surface height, depressing isopycnals, and caus-  
217 ing inshore surface flow and offshore bottom flow along Greenland’s southeastern coast  
218 – to a relaxation of that build-up or, more commonly, to upwelling conditions, which leads  
219 to the opposite oceanic response (Håvik & Våge, 2018). Fjord outflow visible at the sur-

220 face during the intrusions (Figure 2a) - which are consistent with fjord intermediary flow  
221 driven by coastal upwelling - support this notion (Straneo et al., 2010; Jackson et al.,  
222 2014). Only two intrusions occurred under persistent, weaker downwelling-favorable winds,  
223 though, they both coincided with cyclones passing over the Irminger Sea and one was  
224 associated with an  $\sim 30$  cm drop in SSH. Other influences such as tides and cyclonic ed-  
225 dies propagating along the continental slope (Bruce, 1995; Magaldi et al., 2011; Brear-  
226 ley et al., 2012; Sutherland & Pickart, 2008) may moderate intrusions, but we rule them  
227 out as primary forcing mechanisms because of the frequencies mismatch between those  
228 phenomena (sub-daily to 1-2 days) and the less frequent AW intrusions ( $>2$  days). We  
229 also rule out piteraq, which rarely coincide with AW intrusions (11%; see Table S1) and  
230 do so only when upwelling-favorable wind conditions simultaneously occurred offshore.

231 The reanalysis and moored ocean records confirm the close linkages between the  
232 intrusions, alongshore wind stress, SSH, and inshore ocean warming. Alongshore wind  
233 stress and SSH records have a strong positive correlation ( $r=0.36$ ,  $p<0.001$ ) and both  
234 had significant negative correlations with the mooring records from the shelf at 290 m,  
235 mid-fjord at 250 m and mid-fjord at 350 m depth ( $r=-0.19$  to  $-0.24$  with wind stress,  $r=\sim-$   
236  $0.32$  with SSH,  $p<0.001$ ; see Supplementary Information). These negative correlations  
237 are consistent with a downwelling-to-upwelling switch in coastal conditions. It is diffi-  
238 cult to distinguish between temperature changes associated with the heaving of isopy-  
239 cnals vertically in the water column and lateral advection of warm water into the fjord  
240 without closer examination of the changes across intrusion events.

241 To examine the effect of the shift from downwelling to upwelling favorable winds,  
242 we create composites of the atmospheric and ocean variability during the intrusions to  
243 identify linkages (Figure 2c). To build the composite, we normalized each of the param-  
244 eters by their mean over the period spanning 300 hours before and after the times of downwelling-  
245 to-upwelling wind shift that occurs within the 24 hours preceding the imagery-indicated  
246 intrusion events. We then average across all identified intrusions events.

247 Both the satellite and mooring observations show a shift to warmer ocean temper-  
248 atures on the shelf and in the fjord that persists for at least eight days after the intru-  
249 sions (Figure 2c). MODIS brightness temperatures revealed surface water temperatures  
250 (Figure S1) within the intrusions could be  $\sim 4^\circ\text{C}$  warmer than those in the EGCC and  
251 fjord, similar to AW temperatures within the IC. Further, when we use mean temper-

252 ature differences from the 4 days before and 4 days after the events ( $\Delta T_{4,-4}$ ) as an in-  
253 dication of temperature change, the intrusions corresponded with significant warming  
254 at the shelf mooring ( $0.71\pm 0.13^\circ\text{C}$ ) and mid-fjord moorings at 250 m ( $0.44\pm 0.13^\circ\text{C}$ ), 350  
255 m ( $0.24\pm 0.08^\circ\text{C}$ ), and 400 m ( $0.08\pm 0.05^\circ\text{C}$ ), though not at 550 m ( $0.01\pm 0.03^\circ\text{C}$ ). The  
256 warming trend held for  $\Delta T_{4:8,-4:8}$  (difference between temperatures averaged over 4-  
257 8 days before and 4-8 days after the wind events) at all moorings between 250 and 400  
258 m (shelf:  $0.31\pm 0.18^\circ\text{C}$ ; mid-fjord 250m:  $0.30\pm 0.19^\circ\text{C}$ ; mid-fjord 350m:  $0.17\pm 0.09^\circ\text{C}$ ; mid-  
259 fjord 400m:  $0.09\pm 0.07^\circ\text{C}$ ). These indicate that the intrusions led to sustained warming  
260 in the upper AW layer (250-400 m deep; Figure S1) through laterally transporting warm  
261 AW to the shelf and fjord, rather than merely producing the vertical heaving of isopy-  
262 cnals (Jackson et al., 2014).

263 Our finding that the AW intrusions produce significant warming inshore at the sur-  
264 face and at depth indicates enhanced upwelling and shoreward transport of AW along  
265 Sermilik Trough. Subsurface warming at the fjord mouth and mid-fjord are consistent  
266 with our satellite-based findings that the intrusions drive warm surface water inshore to-  
267 ward Sermilik Fjord. The subsurface warming within the fjord show that this water is  
268 also transported into the fjord at depths of 250 and 400 m and potentially the entire AW  
269 layer. Further, the co-occurrence of shoreward flow in the Sermilik Trough with the shift  
270 in alongshore winds and SSH align with the finding of Zhang and Lentz (2017) that upwelling-  
271 favorable winds (Hampson, 2020) or a relaxation of strong downwelling-favorable winds  
272 can drive strong onshore cross-shelf flow in a shelf valley (see below).

273 While the majority of all intrusions (79% for the +4-day window, 55% for the 4  
274 to 8-day window) resulted in warming on the shelf, exceptions exist. On an event-by-  
275 event basis, sustained ocean warming occurred frequently (92% on the shelf and approx-  
276 imately two-thirds in the fjord) when the EGCC was narrow ( $<61\pm 14$  km), and less fre-  
277 quently (42% on the shelf and  $\sim 35\%$  in the fjord) when the EGCC was wider. These find-  
278 ings indicate that the width of the EGCC and therefore transport (see Supplemental In-  
279 formation), moderate AW intrusion inshore, which is consistent with previous research  
280 finding that EGCC width increases the dilution of AW as it crosses the continental shelf  
281 (Snow et al., 2021). Other factors that may impact the recorded warming signals inshore  
282 include variability in source water temperature or a rapid temperature fluctuation ob-  
283 scuring our temperature metric. For instance, a coastal downwelling occurring 4-8 days  
284 after an intrusion would be considered by our analysis as a cooling event.

## Discussion

Shoreward flow of AW replenishes heat at depth within the interior of the continental shelf and the fjords along SE Greenland, and herein we have described an along-shore wind mechanism that actively pumps AW inshore along the trough leading to Sermilik Fjord. We show that upwelling-favorable wind events drive AW upwelling and inflow toward Sermilik Fjord within the trough (Figure 2, S1). These conditions are most often driven by cyclones (LP systems) and, less frequently, anti-cyclones (HP). 79% of the identified intrusions lead to subsurface warming at moorings near the fjord mouth (290 m) and >50% of the intrusions lead to warming mid-fjord (250 m and 400 m). These increase the amount of heat flowing toward Helheim Glacier.

We provide a holistic description of the AW intrusion events that links wind-driven fjord and continental shelf processes (Figure 1). During downwelling-favorable winds (Figure 1b), the EGCC flows faster (Le Bras et al., 2018), isopycnals depress, and the sea surface raises  $O(15\text{cm})$  toward the coastline on the shelf (Jackson et al., 2014; Harden et al., 2014; Håvik & Våge, 2018). Water along the coast experiences a negative density anomaly and positive bottom pressure anomaly (indicating a positive sea-surface height anomaly) (Harden et al., 2014) that propagates up-fjord (Jackson et al., 2014). Within the fjord, the PW layer thickens as water flows in at the surface, isopycnals heave downwards, the subsurface warm layer thins as AW flows out of the fjord, and the sea surface rises (Straneo et al., 2010; Jackson et al., 2014). When this prevailing wind mode transitions to upwelling-favorable winds (Figure 1c), the fjord and shelf experience an opposite effect, lifting warm dense AW onto the shelf, driving a shore-ward flow of the AW, and causing PW surface outflow from the fjord and coast (Jackson et al., 2014; Håvik & Våge, 2018). This upwelling response can eject freshwater and sea ice off the continental shelf on the surface (Oltmanns et al., 2014; Håvik & Våge, 2018).

We propose that the Sermilik Trough bathymetry facilitates the onshore intrusion of AW. It results from asymmetric responses of the trough circulation to the ambient along-shelf flows of opposite directions when the Rossby number,  $Ro=U/(fL)$ , of the trough flow is  $O(1)$  (Lentz et al., 2014; Zhang & Lentz, 2017; Hampson, 2020). Here,  $U$  is a scale of the along-shelf flow,  $f$  the Coriolis Parameter, and  $L$  a length scale of the trough. The observed onshore intrusion of the AW along the northeastern flank of the Sermilik Trough is consistent with upwelling flow on upstream canyon slopes (Allen & Hickey, 2010; She

317 & Klinck, 2000; Zhang & Lentz, 2017). During upwelling-favorable winds or sudden re-  
318 duction in downwelling-favorable winds, water along the northeastern flank of the trough  
319 upwells and flows shore-ward throughout the entire water column, lifting dense AW from  
320 the continental slope toward Sermilik Fjord (Figure 1). This onshore flow at the trough  
321 is either a part of a steady standing coastal-trapped wave that is excited at the trough  
322 and then arrested by the northeastward shelf flow, or a transient consequence of the ex-  
323 cessive onshore pressure gradient force associated with the greater water depth in the  
324 trough (Allen & Hickey, 2010). During downwelling-favorable winds, enhancement of the  
325 offshore flow in a canyon/trough is minimum (Allen & Madron, 2009; Lentz et al., 2014),  
326 consistent with topographically generated coastal-trapped waves propagating freely down-  
327 stream (to the southwest in this case) away from the trough. Therefore, downwelling-  
328 and upwelling-favorable winds do not drive equivalent opposing flows along the trough  
329 and oscillatory along-shelf winds can generate localized net onshore inflow in the trough.  
330 The intrusion transports the offshore warm water shoreward into the fjord to alter wa-  
331 ter properties (Håvik & Våge, 2018) in a way that is not diminished during the subse-  
332 quent return of the winds to downwelling-favorable (Figure 2f-h). For this reason, even  
333 if the intruding AW is not advected into the fjord immediately, each upwelling event can  
334 bring some amount of AW onto the shelf nearer to shore that can be delivered into the  
335 fjord and enhance warming there during subsequent events (Kämpf, 2006; Fraser et al.,  
336 2018). During weak wind events, the oscillatory shelf flows are weak with a low Rossby  
337 number (Kämpf, 2009; Lentz et al., 2014), and would not produce net onshore intrusion  
338 of the offshore warm AW. This explains why only some wind-driven intermediary cir-  
339 culation within Sermilik Fjord results in advection of warm waters into the fjord (Jackson  
340 et al., 2014, 2018).

341 Our observations in Sermilik Trough of the appearance of warm water at the sur-  
342 face (upwelling and inflow), at depth (warming from inflow at depth), and the timing  
343 of the appearance (<1 day lag with upwelling-favorable winds) is consistent with bathymetrically-  
344 induced localized onshore intrusion flow of warm AW. A back-of-the-envelope estimate  
345 based on the observed warm water surface signals in MODIS indicates that the intru-  
346 sion velocities in the cross-shelf (along-trough) direction is at least 0.13-0.19 m/s. While  
347 we find good agreement with previous studies (She & Klinck, 2000; Kämpf, 2007; Lentz  
348 et al., 2014; Zhang & Lentz, 2017), those environments (e.g., Hudson Shelf Valley) dif-  
349 fer from the Sermilik system where the EGCC may slow down at times, but not always

350 reverse, during upwelling-favorable winds (Sutherland & Pickart, 2008), which likely sup-  
351 presses the coastal-trapped waves. Future work to model the Sermilik system (i.e., a non-  
352 linear trough carved into an undulating continental shelf that leads to a fjord where there  
353 is a background current and strong stratification) would be needed to confirm our find-  
354 ings.

355 AW inflow into the fjord likely results from the concurrent wind-driven interme-  
356 diary circulation within the fjord. During the intrusions, we observe intermediary cir-  
357 culation as outflow at the surface, which results from the relaxation of downwelling-favorable  
358 winds and/or the onset of upwelling-favorable winds. This outflow indicates the drain-  
359 ing of PW out of the fjord at the surface, which corresponds with a compensating AW  
360 inflow of at depth (Stigebrandt, 1981; Klinck et al., 1981; Straneo et al., 2010). Inter-  
361 mediary circulation explains the advection of warm water - that leads to subsurface warm-  
362 ing at multiple depths within the fjord ( $\Delta T_{4:8,-4:8}$  is  $0.30\pm 0.19^\circ\text{C}$  at 250 m,  $0.17\pm 0.09^\circ\text{C}$   
363 at 350 m, and  $0.09\pm 0.07^\circ\text{C}$  at 400 m) - into Sermilik Fjord toward Helheim Glacier dur-  
364 ing AW intrusions.

365 While wind-driven intrusions advect AW inshore, the EGCC likely serves as a bar-  
366 rier to AW intrusions, both by increasing the physical distance that AW must travel to  
367 reach Sermilik Fjord, and by enhancing ambient shelf stratification that suppresses in-  
368 shore intrusion flow in the surface layer. Narrowing of the EGCC allows a more efficient  
369 intrusion of AW onto the shelf by reducing the distance AW must travel to reach the fjord  
370 and the extent to which the water dilutes along the way (Snow et al., 2021). Consistent  
371 with enhanced temperature variability observed at the subsurface shelf mooring ( $r^2=0.40$ ;  
372 Figure S3), a wider EGCC seasonally also coincides with greater transport and increased  
373 stratification of the deeper water layers along the inner shelf (see Supplementary Infor-  
374 mation). Modeling suggests that strong stratification creates a lid over upwelling within  
375 the canyon and that isopycnals tend to squeeze together above the canyon below the sur-  
376 face layer (Ramos-Musalem & Allen, 2019). A deeper pycnocline suppresses the verti-  
377 cal extent of the bathymetrical influence and, thus, reduces the chance of upwelling flow  
378 reaching the surface. This vertical suppression of the intrusions would limit our ability  
379 to observe them, and restrict the depth range that AW is transported toward the head  
380 of the trough. Greater sea ice concentrations within the EGCC also decouples wind and  
381 surface ocean stresses over the trough, which we speculate would reduce or completely  
382 diminish the intensity of the inflow, though this has not been tested. While greater in-

fluence by the EGCC likely suppresses intrusions, we note that a lack of surface expression does not preclude the intrusions from still occurring at depth (Figure 1c).

We further speculate that greater wind forcing is required to produce intrusions and, thus, enhanced inshore heat transport when the EGCC widens and deepens. Simple-model results suggest that intrusions resulting from upwelling-favorable winds intensify throughout the first 24 hours and remain at these elevated velocities as long as the winds persisted (Zhang & Lentz, 2017). Based on water velocities during the intrusions and the time over which they develop, this would suggest that the strength and duration of an upwelling alongshore wind configuration could greatly affect overall transport of AW during an event. Stratification also diffuses over time by vertical turbulence as upwelling continues (Ramos-Musalem & Allen, 2019), making it more likely for the intrusion to extend upwards in the water column with time. Differences in wind event duration and magnitude or EGCC width during an intrusion likely regulate when the wind events effectively transport AW into the fjord. Offshore AW temperature variability and the depth of inflow also likely moderates whether warming or cooling is observed inshore and within the fjord (Fraser et al., 2018).

Herein we show that many wind-driven intrusions result in warm offshore water being pumped onto the continental shelf and sometimes into Sermilik Fjord. If more frequent upwelling-favorable wind events and less freshwater transport within the EGCC were to occur, this would be expected to lead to higher volumes of AW, and heat, flushing onto the shelf and into Sermilik Fjord. Greater cyclone activity, specific high pressure blocking patterns, and a high NAO index, which relates to storm variability in southeastern Greenland (Harden et al., 2011; Straneo & Heimbach, 2013), could all make intrusions more common. Further, weakening of the EGCC as a result of reduced freshwater and sea ice transport out of the Arctic (Harden et al., 2014), enhanced ejection of PW off the continental shelf, and runoff/iceberg calving from the Greenland Ice Sheet (Sutherland & Pickart, 2008) will reduce the dilution of AW as it crosses the continental shelf and make southeast Greenland fjords more susceptible to warm water inflow (Murray et al., 2010; Snow et al., 2021). Models may be able to predict anomalously high heat transport years using this improved understanding of the linkage between subsurface water temperatures, EGCC width/transport, and intrusion-favorable wind events. As has been demonstrated herein, a better understanding of deep-water heat transport changes that may directly feed into Sermilik Fjord and bring heat to Helheim Glacier both pro-

416 jected into the past and future has substantial implications for pinpointing the role of  
417 the ocean in glacier change. Intrusions of this nature may also occur to varying extents  
418 at other glacier systems around Greenland, such as Kangerdlugssuaq Glacier (Fraser et  
419 al., 2018), which could make it an important mechanism for regulating large-scale ice sheet  
420 dynamical mass loss.

## 421 **Acknowledgments**

422 We gratefully acknowledge the National Aeronautics and Space Administration (NASA),  
423 the U.S. National Science Foundation (NSF), and the Cooperative Institute for Research  
424 in Environmental Sciences (CIRES). This work was supported by NASA Headquarters  
425 under a NASA Earth and Space Science Fellowship Program – Grant (NNX16AO33H).  
426 This material is also based upon work supported by the NSF Graduate Research Fel-  
427 lowship Program under grant DGE1650115. Any opinions, findings, and conclusions or  
428 recommendations expressed in this material are those of the authors and do not neces-  
429 sarily reflect the views of the NSF. We thank Kathleen Bogan (CIRES) for her artistic  
430 design of Figure 1b,c. Processed data used in this manuscript is permanently archived  
431 at the Arctic Data Center (doi:—). The Python Jupyter Notebook processing and anal-  
432 ysis code is available at ---. Users of the code should contact the author to ensure rea-  
433 sonable applications of the method. The Sermilik Fjord mouth mooring data used in this  
434 paper is available at the National Oceanographic Data Center ([https://data.nodc.noaa](https://data.nodc.noaa.gov/cgi-bin/iso?id=gov.noaa.nodc:0127325)  
435 [.gov/cgi-bin/iso?id=gov.noaa.nodc:0127325](https://data.nodc.noaa.gov/cgi-bin/iso?id=gov.noaa.nodc:0127325) and [0127320](https://data.nodc.noaa.gov/cgi-bin/iso?id=gov.noaa.nodc:0127320)). Sea surface height data  
436 was provided by B. Harden. Level 2 MODIS visible and thermal infrared imagery can  
437 be found at [search.earthdata.nasa.gov](https://search.earthdata.nasa.gov), and ECMWF ERA-5 data is located at [www.ecmwf.int](https://www.ecmwf.int).  
438 Thanks also go to the two reviewers for their comments that greatly improved the qual-  
439 ity of this paper.

## 440 **References**

- 441 Allen, S. E., & Hickey, B. M. (2010). Dynamics of advection-driven upwelling over  
442 a shelf break submarine canyon. *Journal of Geophysical Research: Oceans*  
443 (1978–2012), 115(C8). doi: 10.1029/2009jc005731
- 444 Allen, S. E., & Madron, X. D. d. (2009). A review of the role of submarine canyons  
445 in deep-ocean exchange with the shelf. *Ocean Science*, 5(4), 607–620. doi: 10  
446 .5194/os-5-607-2009

- 447 Andresen, C. S., Straneo, F., Ribergaard, M. H., Bjørk, A. A., Andersen, T. J., Kui-  
 448 jpers, A., . . . Ahlstrøm, A. P. (2012). Rapid response of Helheim Glacier in  
 449 Greenland to climate variability over the past century. *Nature Geoscience*,  
 450 5(1), 37–41. doi: 10.1038/ngeo1349
- 451 Brearley, J. A., Pickart, R. S., Valdimarsson, H., Jonsson, S., Schmitt, R. W., &  
 452 Haine, T. W. N. (2012). The East Greenland boundary current system south  
 453 of Denmark Strait. *Deep Sea Research Part I: Oceanographic Research Papers*,  
 454 63, 1–19. doi: 10.1016/j.dsr.2012.01.001
- 455 Bruce, J. G. (1995). Eddies southwest of the Denmark Strait. *Deep Sea Re-*  
 456 *search Part I: Oceanographic Research Papers*, 42(1), 13–29. doi: 10.1016/0967  
 457 -0637(94)00040-y
- 458 Copernicus Climate Change Service. (2017). *ERA5: Fifth generation of ECMWF*  
 459 *atmospheric reanalyses of the global climate*. <https://cds.climate.copernicus.eu>.  
 460 (Accessed: 2018-11-04)
- 461 Cowton, T., Sole, A., Nienow, P., Slater, D., & Hanna, E. (2016). Controls on the  
 462 transport of oceanic heat to Kangerdlugssuaq Glacier, East Greenland. *Journal*  
 463 *of Glaciology*, 62(236), 1167–1180. doi: 10.1017/jog.2016.117
- 464 Crawford, A. D., Alley, K. E., Cooke, A. M., & Serreze, M. C. (2020). Synoptic  
 465 Climatology of Rain-on-Snow Events in Alaska Synoptic Climatology of Rain-  
 466 on-Snow Events in Alaska. *Monthly Weather Review*, 148(3), 1275–1295. doi:  
 467 10.1175/mwr-d-19-0311.1
- 468 Crawford, A. D., & Serreze, M. C. (2016). Does the Summer Arctic Frontal Zone  
 469 Influence Arctic Ocean Cyclone Activity? *Journal of Climate*, 29(13), 4977–  
 470 4993. doi: 10.1175/jcli-d-15-0755.1
- 471 Enderlin, E. M., Howat, I. M., Jeong, S., Noh, M., Angelen, J. H., & van den  
 472 Broeke, M. R. (2014). An improved mass budget for the Greenland ice sheet.  
 473 *Geophysical Research Letters*, 41(3), 866–872. doi: 10.1002/2013GL059010
- 474 Fraser, N. J., Inall, M. E., Magaldi, M. G., Haine, T. W. N., & Jones, S. C. (2018).  
 475 Wintertime Fjord-Shelf Interaction and Ice Sheet Melting in Southeast Green-  
 476 land. *Journal of Geophysical Research: Oceans*, 123(12), 9156–9177. doi:  
 477 10.1029/2018jc014435
- 478 Hampson, P. (2020). *Glacial Troughs Eject Wind-Driven Shelf Circulation to the*  
 479 *Slope* (Unpublished doctoral dissertation).

- 480 Harden, B., Renfrew, I., & Petersen, G. (2011). A Climatology of Wintertime Bar-  
481 rier Winds off Southeast Greenland. *Journal of Climate*, *24*(17), 4701–4717.  
482 doi: 10.1175/2011JCLI4113.1
- 483 Harden, B., Straneo, F., & Sutherland, D. (2014). Moored observations of  
484 synoptic and seasonal variability in the East Greenland Coastal Cur-  
485 rent. *Journal of Geophysical Research: Oceans*, *119*(12), 8838–8857. doi:  
486 10.1002/2014JC010134
- 487 Holland, D. M., Thomas, R. H., Young, B. d., Ribergaard, M. H., & Lyberth, B.  
488 (2008). Acceleration of Jakobshavn Isbræ triggered by warm subsurface ocean  
489 waters. *Nature Geoscience*, *1*, 659. doi: 10.1038/ngeo316
- 490 Howat, I. M., Joughin, I., Fahnestock, M., Smith, B., & Scambos, T. (2008).  
491 Synchronous retreat and acceleration of southeast Greenland outlet glaciers  
492 2000–06: Ice dynamics and coupling to climate. *Journal of Glaciology*,  
493 *54*(187).
- 494 Håvik, L., & Våge, K. (2018). Wind-Driven Coastal Upwelling and Downwelling  
495 in the Shelfbreak East Greenland Current. *Journal of Geophysical Research:*  
496 *Oceans*, *123*(9), 6106–6115. doi: 10.1029/2018jc014273
- 497 IMBIE Team, T. (2019). Mass balance of the Greenland Ice Sheet from 1992 to  
498 2018. *Nature*. doi: 10.1038/s41586-019-1855-2
- 499 Jackson, R. H., Lentz, S. J., & Straneo, F. (2018). The Dynamics of Shelf Forcing in  
500 Greenlandic Fjords. *Journal of Physical Oceanography*, *48*(11), 2799–2827. doi:  
501 10.1175/jpo-d-18-0057.1
- 502 Jackson, R. H., & Straneo, F. (2016). Heat, Salt, and Freshwater Budgets for a  
503 Glacial Fjord in Greenland. *Journal of Physical Oceanography*, *46*(9), 2735–  
504 2768. doi: 10.1175/JPO-D-15-0134.1
- 505 Jackson, R. H., Straneo, F., & Sutherland, D. A. (2014). Externally forced fluctu-  
506 ations in ocean temperature at Greenland glaciers in non-summer months. *Na-*  
507 *ture Geoscience*, *7*(7), 503–508. doi: 10.1038/ngeo2186
- 508 Johannessen, O. M., Korablev, A., Miles, V., Miles, M. W., & Solberg, K. E. (2011).  
509 Interaction Between the Warm Subsurface Atlantic Water in the Sermilik  
510 Fjord and Helheim Glacier in Southeast Greenland. *Surveys in Geophysics*,  
511 *32*(4-5), 387. doi: 10.1007/s10712-011-9130-6
- 512 Klinck, J. M., O'Brien, J. J., & Svendsen, H. (1981). A Simple Model of Fjord and

- 513 Coastal Circulation Interaction. *Journal of Physical Oceanography*, 11(12),  
514 1612–1626.
- 515 Kämpf, J. (2006). Transient wind-driven upwelling in a submarine canyon: A  
516 process-oriented modeling study. *Journal of Geophysical Research: Oceans*  
517 (1978–2012), 111(C11). doi: 10.1029/2006jc003497
- 518 Kämpf, J. (2007). On the magnitude of upwelling fluxes in shelf-break canyons.  
519 *Continental Shelf Research*, 27(17), 2211–2223. doi: 10.1016/j.csr.2007.05.010
- 520 Kämpf, J. (2009). On the Interaction of Time-Variable Flows with a Shelfbreak  
521 Canyon. *Journal of Physical Oceanography*, 39(1), 248–260. doi: 10.1175/  
522 2008jpo3753.1
- 523 Le Bras, I., Straneo, F., Holte, J., & Holliday, P. N. (2018). Seasonality of Freshwa-  
524 ter in the East Greenland Current System From 2014 to 2016. *Journal of Geo-*  
525 *physical Research: Oceans*. doi: 10.1029/2018JC014511
- 526 Lentz, S. J., Butman, B., & Harris, C. (2014). The vertical structure of the circu-  
527 lation and dynamics in Hudson Shelf Valley. *Journal of Geophysical Research:*  
528 *Oceans*, 119(6). doi: 10.1002/2014jc009883
- 529 Magaldi, M. G., Haine, T. W. N., & Pickart, R. S. (2011). On the Nature and Vari-  
530 ability of the East Greenland Spill Jet: A Case Study in Summer 2003\*. *Jour-*  
531 *nal of Physical Oceanography*, 41(12), 2307–2327. doi: 10.1175/jpo-d-10-05004  
532 .1
- 533 Millan, R., Rignot, E., Mouginot, J., Wood, M., Bjørk, A., & Morlighem, M. (2018).  
534 Vulnerability of Southeast Greenland Glaciers to Warm Atlantic Water From  
535 Operation IceBridge and Ocean Melting Greenland Data. *Geophysical Research*  
536 *Letters*, 45(6), 2688–2696. doi: 10.1002/2017GL076561
- 537 Morlighem, M., Williams, C. N., Rignot, E., An, L., Arndt, J. E., Bamber, J. L., . . .  
538 Zinglensen, K. B. (2017). BedMachine v3: Complete Bed Topography and  
539 Ocean Bathymetry Mapping of Greenland From Multibeam Echo Sounding  
540 Combined With Mass Conservation. *Geophysical research letters*, 44(21),  
541 11051–11061. doi: 10.1002/2017gl074954
- 542 Mouginot, J., Rignot, E., Bjørk, A. A., van den Broeke, M., Millan, R., Morlighem,  
543 M., . . . Wood, M. (2019). Forty-six years of Greenland Ice Sheet mass balance  
544 from 1972 to 2018. *Proceedings of the National Academy of Sciences*, 116(19),  
545 9239–9244. doi: 10.1073/pnas.1904242116

- 546 Mouginit, J., Rignot, E., Scheuchl, B., Fenty, I., Khazendar, A., Morlighem, M.,  
547 ... Paden, J. (2015). Fast retreat of Zachariæ Isstrøm, northeast Greenland.  
548 *Science*, *350*(6266), 1357–1361. doi: 10.1126/science.aac7111
- 549 Murray, T., Scharrer, K., James, T., Dye, S., Hanna, E., Booth, A., ... Huybrechts,  
550 P. (2010). Ocean regulation hypothesis for glacier dynamics in southeast  
551 Greenland and implications for ice sheet mass changes. *Journal of Geophysical*  
552 *Research: Earth Surface (2003–2012)*, *115*(F3). doi: 10.1029/2009JF001522
- 553 Oltmanns, M., Straneo, F., Moore, G., & Mernild, S. (2014). Strong Downslope  
554 Wind Events in Ammassalik, Southeast Greenland. *Journal of Climate*, *27*(3),  
555 977–993. doi: 10.1175/JCLI-D-13-00067.1
- 556 Ramos-Musalem, K., & Allen, S. E. (2019). The impact of locally-enhanced verti-  
557 cal diffusivity on the cross-shelf transport of tracers induced by a submarine  
558 canyon The impact of locally-enhanced vertical diffusivity on the cross-shelf  
559 transport of tracers induced by a submarine canyon. *Journal of Physical*  
560 *Oceanography*, *49*(2), 561–584. doi: 10.1175/jpo-d-18-0174.1
- 561 Rudels, B., Fahrback, E., Meincke, J., Budéus, G., & Eriksson, P. (2002). The East  
562 Greenland Current and its contribution to the Denmark Strait overflow. *ICES*  
563 *Journal of Marine Science*, *59*(6), 1133–1154. doi: 10.1006/jmsc.2002.1284
- 564 Sciascia, R., Cenedese, C., Nicolì, D., Heimbach, P., & Straneo, F. (2014). Im-  
565 pact of periodic intermediary flows on submarine melting of a Greenland  
566 glacier. *Journal of Geophysical Research: Oceans*, *119*(10), 7078–7098. doi:  
567 10.1002/2014jc009953
- 568 She, J., & Klinck, J. M. (2000). Flow near submarine canyons driven by constant  
569 winds. *Journal of Geophysical Research: Oceans*, *105*(C12), 28671–28694. doi:  
570 10.1029/2000jc900126
- 571 Smith, B., Fricker, H. A., Gardner, A. S., Medley, B., Nilsson, J., Paolo, F. S.,  
572 ... Zwally, H. J. (2020). Pervasive ice sheet mass loss reflects compet-  
573 ing ocean and atmosphere processes. *Science*, *368*(6496), 1239–1242. doi:  
574 10.1126/science.aaz5845
- 575 Snow, T., Straneo, F., Holte, J., Grigsby, S., Abdalati, W., & Scambos, T.  
576 (2021). More than skin deep: sea surface temperature as a means of in-  
577 ferring Atlantic Water variability on the southeast Greenland continental  
578 shelf near Helheim Glacier. *Journal of Geophysical Research: Oceans*. doi:

- 579 <https://www.essoar.org/doi/abs/10.1002/essoar.10503490.1>
- 580 Stigebrandt, A. (1981). A mechanism governing the estuarine circulation in deep,  
581 strongly stratified fjords. *Estuarine, Coastal and Shelf Science*, 13(2), 197–211.  
582 doi: 10.1016/s0302-3524(81)80076-x
- 583 Straneo, F., Curry, R., Sutherland, D., & Hamilton, G. (2011). Impact of fjord dy-  
584 namics and glacial runoff on the circulation near Helheim Glacier. *Nature Geo-*  
585 *science*, 4. doi: 10.1038/ngeo1109
- 586 Straneo, F., Hamilton, G. S., Sutherland, D. A., Stearns, L. A., Davidson, F., Ham-  
587 mill, M. O., . . . Rosing-Asvid, A. (2010). Rapid circulation of warm subtropi-  
588 cal waters in a major glacial fjord in East Greenland. *Nature Geoscience*, 3(3),  
589 182. doi: 10.1038/ngeo764
- 590 Straneo, F., & Heimbach, P. (2013). North Atlantic warming and the re-  
591 treat of Greenland’s outlet glaciers. *Nature*, 504(7478), 36–43. doi:  
592 10.1038/nature12854
- 593 Sutherland, D. A., & Pickart, R. S. (2008). The East Greenland Coastal Current:  
594 Structure, variability, and forcing. *Progress in Oceanography*, 78(1), 58–77.  
595 doi: 10.1016/j.pocean.2007.09.006
- 596 Sutherland, D. A., Straneo, F., & Pickart, R. S. (2014). Characteristics and dy-  
597 namics of two major Greenland glacial fjords. *Journal of Geophysical Research:*  
598 *Oceans*, 119(6), 3767–3791. doi: 10.1002/2013JC009786
- 599 Sutherland, D. A., Straneo, F., Stenson, G. B., Davidson, F., Hammill, M. O., &  
600 Rosing-Asvid, A. (2013). Atlantic water variability on the SE Greenland  
601 continental shelf and its relationship to SST and bathymetry. *Journal of*  
602 *Geophysical Research: Oceans*, 118(2), 847–855. doi: 10.1029/2012JC008354
- 603 Svendsen, H., & Thompson, R. O. R. Y. (1978). Wind-Driven Circulation in a  
604 Fjord. *Journal of Physical Oceanography*, 8(4), 703–712.
- 605 Våge, K., Pickart, R. S., Sarafanov, A., Knutsen, O., Mercier, H., Lherminier, P., . . .  
606 Bacon, S. (2011). The Irminger Gyre: Circulation, convection, and interannual  
607 variability. *Deep Sea Research Part I: Oceanographic Research Papers*, 58(5),  
608 590–614. doi: 10.1016/j.dsr.2011.03.001
- 609 Zhang, W. G., & Lentz, S. J. (2017). Wind-Driven Circulation in a Shelf Valley.  
610 Part I: Mechanism of the Asymmetrical Response to Along-Shelf Winds in  
611 Opposite Directions. *Journal of Physical Oceanography*, 47(12), 2927–2947.

